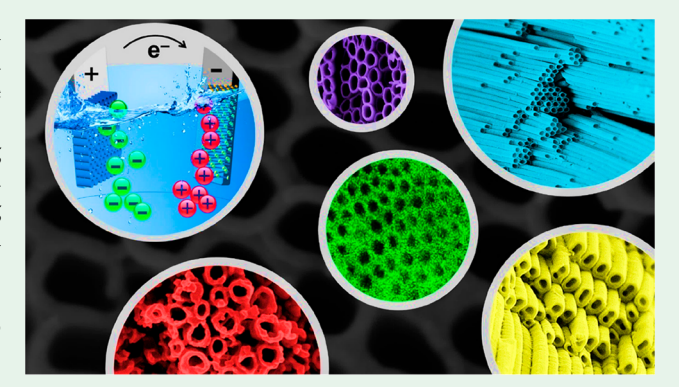
Selective Electrochemical Capture and Release of Heparin Based on Amine-Functionalized Carbon/Titanium Dioxide Nanotube Arrays

Hamed Eskandarloo, Mojtaba Enayati, Mahmood Karimi Abdolmaleki, Mohammad Arshadi, and Alireza Abbaspourrad*

Department of Food Science, College of Agriculture & Life Sciences, Cornell University, 243 Stocking Hall, Ithaca, New York 14853, United States

Supporting Information

ABSTRACT: Heparin (HEP) is a sulfated glycosaminoglycan that is a clinical anticoagulant agent. Commercially derived from porcine intestinal mucosa, HEP is challenging to separate from this complex biological mixture for additional purification. This study aimed to raise the purity of isolated HEP using electrochemical potential to increase its selective capture and release. We demonstrate an electrochemical platform featuring an anode composed of amine-functionalized carbon/titanium dioxide nanotube arrays on titanium foil (Ti/C-TNTAs-NH₂) and a cathode made of expanded graphite. Our results show that Ti and Ti/C-TNTAs control plates do not adsorb HEP, even while applying an external potential to the cell. However, when the Ti/C-TNTAs electrode is modified by 3



aminopropyltriethoxysilane, the terminal NH2 groups provide a high density of positive charges that serve as binding sites, enabling the adsorption of HEP. This attraction is further strengthened by applying an external potential to the anode. Subsequent release of the HEP molecules and regeneration of the Ti/C-TNTAs-NH2 electrode are easily accomplished by applying an anodic potential to the plate, as well as by increasing the concentration of NaCl in solution. This electrochemical system demonstrates the good selectivity of HEP, even within a mixture of other probable interfering species (e.g., bovine serum albumin and chondroitin sulfate). Additionally, it maintains 90.11% of its initial electrosorption efficiency after ten repeated HEP adsorption/desorption cycles, indicating this system's promising stability and reusability for HEP purification.

KEYWORDS: heparin recovery, heparin digestion, electrosorption, selective adsorption, titanium dioxide nanotubes, functionalized nanotubes

INTRODUCTION

Downloaded by CORNELL UNIV at 08:28:32:008 on June 24, 2019 from https://pubs.acs.org/doi/10.1021/acsabm.9b00400.

Heparin (HEP) is a linear long-chain, highly sulfated glycosaminoglycan featuring a high density of negative charges, which is commercially extracted from animal tissue, such as the intestinal mucosa of pigs.2 HEP serves various clinical applications, particularly as an anticoagulant for the treatment of acute coronary syndrome, arterial thrombosis, atrial fibrillation, and pulmonary embolism.3 Unfortunately, only very low concentrations (0.01% w/w) of HEP are isolated from enzymatically digested natural tissue.4 Therefore, an additional separation step is required for the selective capture of HEP from other contaminating compounds present in the digestion mixture (e.g., other glycosaminoglycans, proteins, nucleic acids, etc.) prior to additional refinement.⁴

Several methods for the selective separation of HEP from raw materials have been reported, most of which are based on the ion-exchange technique. In this method, primary amines/ quaternary ammonium groups are used to selectively form an insoluble complex with HEP molecules,4 exploiting the unusually high density of negative charges found on the HEP molecule, which distinguishes it from other compounds

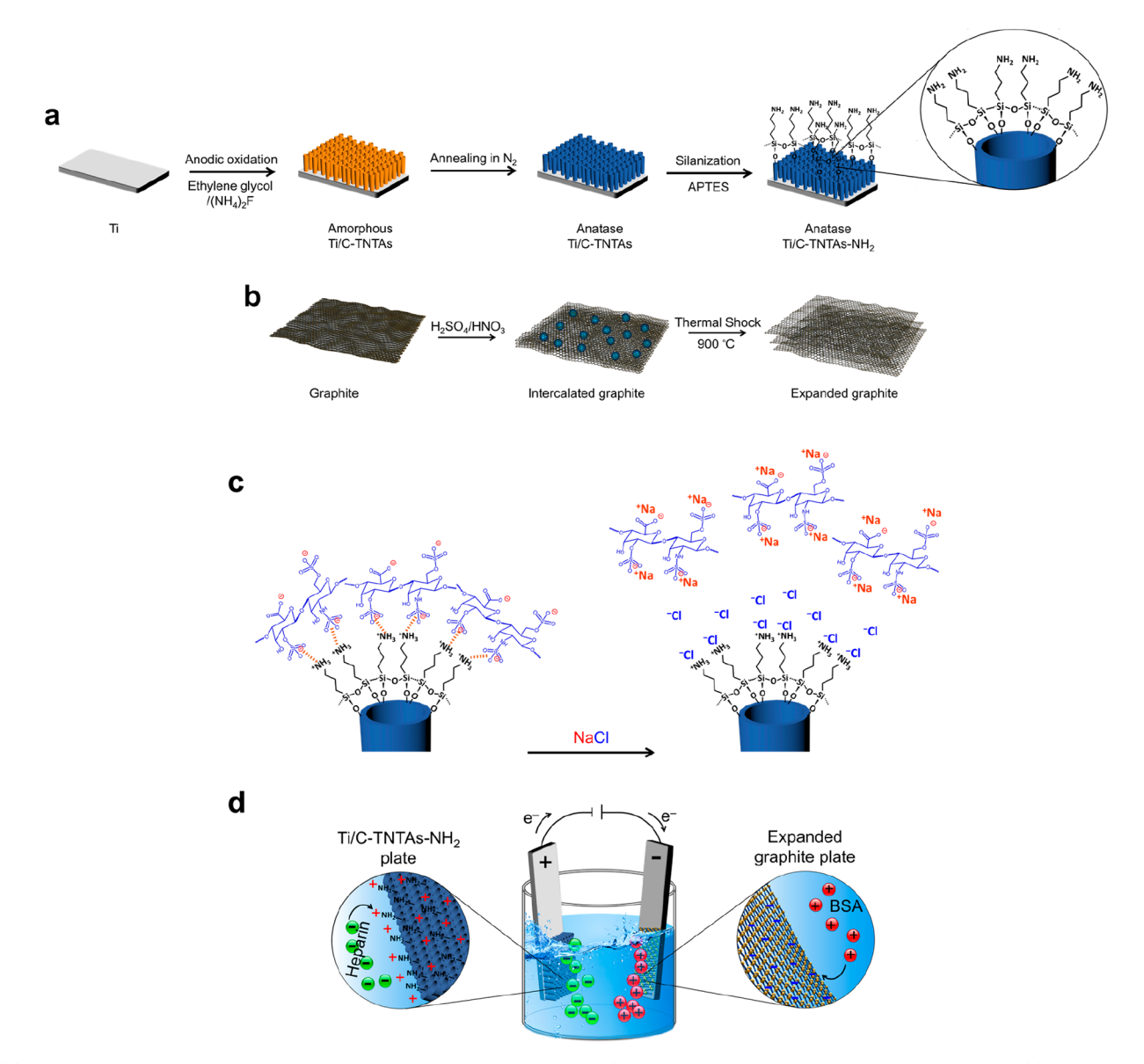
found in the digestion mixture. In this manner, HEP can be separated by robust charge-based cooperative binding,⁵ which has been demonstrated using chitosan and its derivatives, 5-7 polymer-based materials, 8,9 hydroxyapatite, 10 and clay nanotubes. 11,12 However, the low selectivity in HEP recovery and the high impurity content in the final sample continues to be a major challenge.

Recent attention has been drawn by the development of a new, environmentally safe ion-exchange technique based on electrochemical switching. 13-18 Electrochemical adsorption (i.e., electrosorption) is defined as a polarization or current potential-induced adsorption phenomenon that takes place on the surface of charged electrodes with a high conductivity. 19 In this kind of a system, increasing the adsorption rate and capacity, as well as the reversible capture and release of the target molecules, can be accomplished with the use of fewer chemicals by controlling the potential.²⁰ In addition, the

Received: May 9, 2019 Accepted: May 15, 2019 Published: May 15, 2019



Scheme 1. Schematic Illustration



"(a) Fabrication and post-modification of the Ti/C-TNTAs-NH₂ anode, (b) formation of the expanded graphite cathode, and (c) replacement of HEP molecules adsorbed on the Ti/C-TNTAs-NH₂ electrode using Cl⁻ ions present in the aqueous solution. (d) The electrochemical system, including the anodic Ti/C-TNTAs-NH₂ plate and cathodic expanded graphite, with the suggested mechanism of the electrosorption separation of negatively charged HEP from the positively charged BSA.

adsorbent film can be simply regenerated without the creation of any secondary waste. ²¹ These features make the technology more economical to operate, with the ability to decrease costs even further if renewable energy sources are utilized. ²² The electrosorption technique has been successfully demonstrated to enhance the adsorption capacity of various cations/anions and organic compounds and the industrial use of this technique has been developed. ²³

Nanotubes have received significant attention because of their size-dependent properties and high surface to volume ratios.²⁴ In recent studies, it has been shown that titanium dioxide nanotubes (TNTs) have improved properties compared to any other known form of this material for application in areas such as sensing, photocatalysis, electrophotocatalysis, solar cells, and photovoltaics.²⁵ TNTs have been fabricated by a variety of methods, including sol—gel

processes, alumina templating, seeded growth, and the hydrothermal method. However, of these TNT synthesis methods, the architecture indicating by far the most amazing properties are highly ordered titanium dioxide nanotube arrays (TNTAs) fabricated by anodic oxidation of a titanium foil/plate in a fluoride-containing electrolyte. This approach offers precise control of the nanotube dimensions. Uniform TNTAs of various tube wall thicknesses of 7–34 nm, tube openings of 22–110 nm, and tube lengths of 200–6000 nm can be easily grown by modifying the anodic oxidation parameters. There are multiple case reports giving evidence of the unique properties of the TiO2 nanotube architecture, making them of significant value for scientific research as well as industrial applications. $^{24-26}$

In this work, we propose a new separation platform based on the electrosorption technique to overcome the challenge of low ACS Applied Bio Materials Article

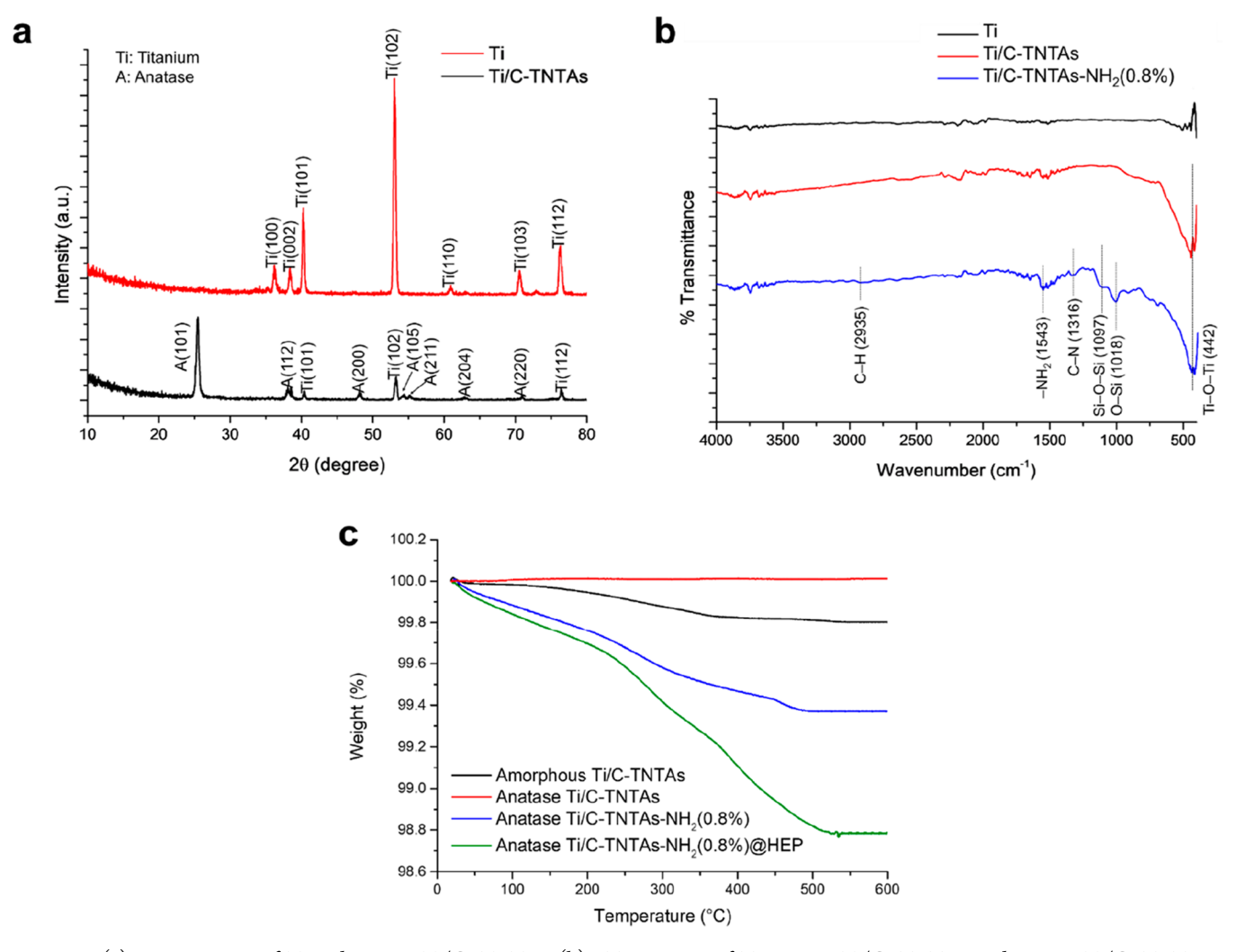


Figure 1. (a) XRD patterns of Ti and anatase Ti/C-TNTAs. (b) FTIR spectra of Ti, anatase Ti/C-TNTAs, and anatase Ti/C-TNTAs-NH₂(0.8%). (c) TGA thermograms of amorphous Ti/C-TNTAs, anatase Ti/C-TNTAs, anatase Ti/C-TNTAs-NH₂(0.8%), and anatase Ti/C-TNTAs-NH₂(0.8%)@HEP.

selectivity of conventional absorbents used in the recovery of HEP. We demonstrate an electrochemical cell featuring an anode made of amine-functionalized carbon/titanium dioxide nanotube arrays on titanium foil (Ti/C-TNTAs-NH₂) and a cathode of expanded graphite, which we employ to boost the selective capture and release of HEP via the application of electrochemical potential. We evaluated the efficiency and selectivity of this electrochemical cell for the capture of HEP in a simulated biological mixture also containing bovine serum albumin (BSA) and chondroitin sulfate (CS), as well as a real biological sample composed of enzymatically digested porcine intestinal mucosa. Our findings suggest this electrochemical cell features both a strong selectivity and stability, enabling it to be reused for repeated HEP separation and recovery.

■ RESULTS AND DISCUSSION

Electrochemical Cell Fabrication. To form the anode, amorphous carbon/titanium dioxide nanotube arrays (C-TNTAs) were grown on pretreated Ti foil by anodic oxidation in an ethylene glycol/ammonium fluoride electrolyte (see the Supporting Information for more details). The amorphous Ti/C-TNTAs were then crystallized by annealing in nitrogen at 500 °C (Scheme 1a). Throughout the annealing process, the remaining ethylene glycol in the TNTAs is carbonized, doping

the TNTs,²⁷ which has been shown to increase the inherent conductivity of these materials by changing the band structure. For instance, carbon-doped TNTAs show superb discharge and charge capacities because of the higher electronic conductivity.^{27,28}

The X-ray diffraction (XRD) patterns of the Ti support and the crystallized Ti/C–TNTAs is shown in Figure 1a. The reflections at 2θ of 36.0° , 38.4° , 40.3° , 53.4° , 60.9° , 70.8° , and 76.4° are attributed to the Ti support (JCPDS card no. 44-1294), and reflections at 2θ of 25.5° , 38.3° , 48.2° , 54.4° , 55.2° , 63.0° , and 71.0° are attributed to the anatase phase of TiO₂ (JCPDS card no. 21-1272). The XRD pattern for Ti/C–TNTAs showed that the TNTs are well-crystallized into the anatase crystalline phase. ²⁹

Surface modification of the anatase Ti/C-TNTAs plate was then carried out by first exposing the substrate to water vapor in order to create a high coverage of Ti-OH groups onto the surface of the TNTAs, followed by immersion in dry toluene and the addition of the amine-terminated silane coupling agent (3 aminopropyltriethoxysilane, APTES) at different concentrations (0.4, 0.6, 0.8, 1.00, and 1.20% v/v) under stirring at 60 °C. These series of steps for the anodic oxidation and subsequent thermal treatment and surface modification processes are shown in Scheme 1a. Optical images of the Ti

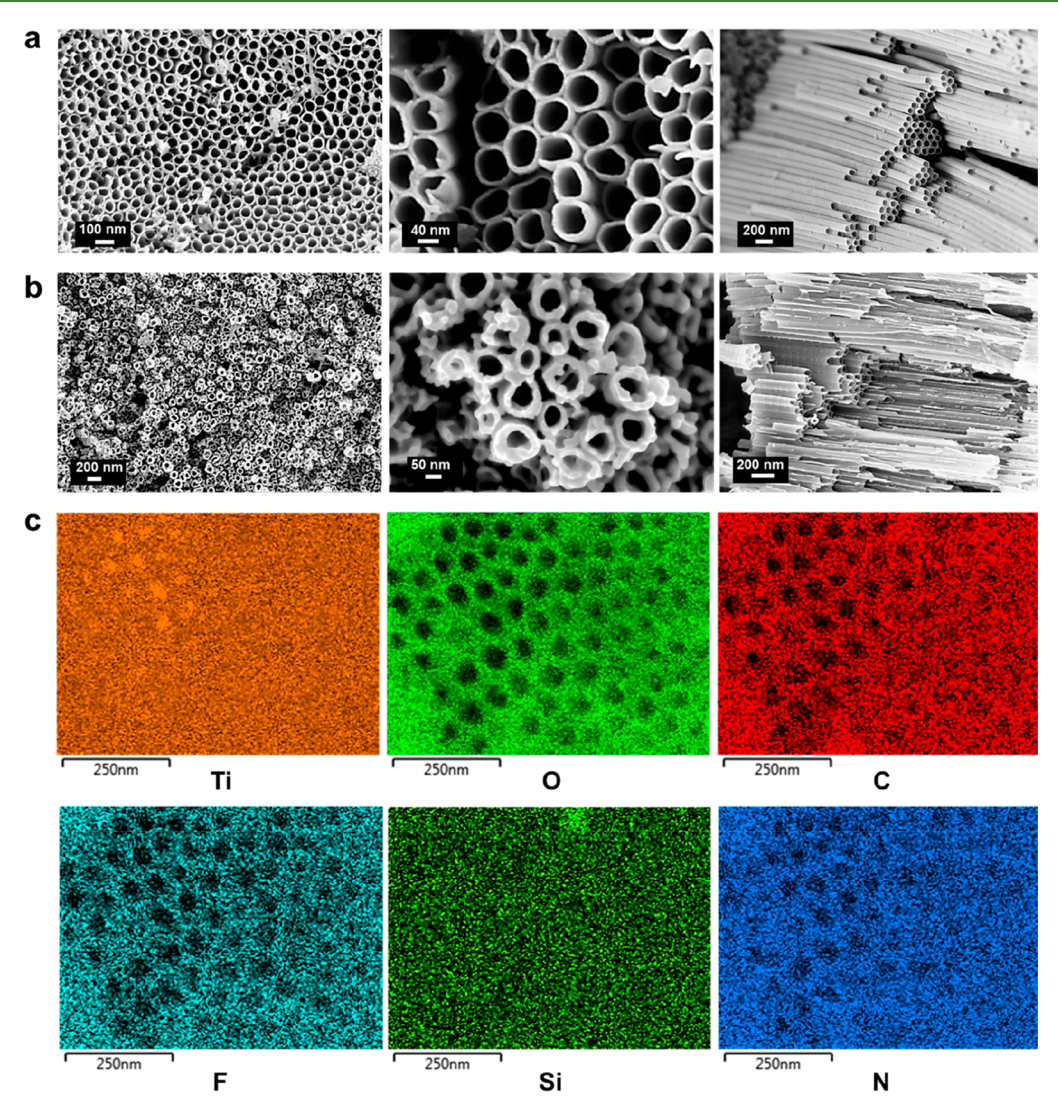


Figure 2. Top-view and cross-sectional SEM images of (a) anatase Ti/C-TNTAs and (b) anatase Ti/C-TNTAs-NH₂(0.8%) at different magnifications. (c) EDX mapping of the anatase Ti/C-TNTAs-NH₂(0.8%) electrode.

foil, amorphous ${\rm Ti/C-TNTAs}$, and anatase ${\rm Ti/C-TNTAs-NH_2(0.8\%)}$ are displayed in Figure S1 (see the Supporting Information). The color of the Ti support changes from silver to white after the TNTA growth on the surface. The color of the amorphous ${\rm Ti/C-TNTAs}$ also changed from white to gray when annealed in nitrogen. Finally, the color transformed to brown after 0.8% APTES modification of the surface.

We studied the Ti plate before and after growth of TNTAs and APTES modification using Fourier transform infrared (FTIR) spectroscopy. FTIR spectra of the Ti support, anatase Ti/C-TNTAs, and anatase $Ti/C-TNTAs-NH_2(0.8\%)$ are shown in Figure 1b. In the FTIR spectra of the anatase Ti/C-TNTAs and anatase Ti/C-TNTAs-NH₂, a broad absorption band appears at 600-400 cm⁻¹, which can be attributed to the Ti-O-Ti bond.³⁰ Compared to the anatase Ti/C-TNTAs, the FTIR spectrum of the anatase Ti/C-TNTAs-NH₂ showed a new absorption band at 1018 cm⁻¹, which we attributed to the stretching vibration of Ti-O-Si, produced by the condensation reaction of Si-OH groups of APTES with the OH groups of the TNTAs.³¹ Moreover, we observed a new band at 1097 cm⁻¹, which can be attributed to the stretching vibration of Si-O-Si, formed by the condensation reaction between Si-OH groups of the APTES. The FTIR spectrum of anatase ${\rm Ti/C-TNTAs-NH_2}$ showed a weak absorption band at 2935 cm⁻¹, which is due to ${\rm (CH_2)_n}$ groups of the APTES. In addition, the weak absorption bands at 1316 and 1543 cm⁻¹ are attributable to the C–N and NH₂ vibrations, signifying the existence of the amino functional groups of APTES on the TNTAs. ¹¹

The fabrication and surface modification of nanotubes were further studied by thermogravimetric analysis (TGA). Figure 1c displays the TGA results in the range from 20 to 600 °C for the amorphous Ti/C-TNTAs, anatase Ti/C-TNTAs, and anatase Ti/C-TNTAs-NH₂(0.8%) before and after HEP adsorption (Ti/C-TNTAs-NH₂(0.8%)@HEP). There is a 0.2% weight loss associated with the amorphous Ti/C-TNTAs, which most likely is due to any remaining ethylene glycol inside the nanotubes during the anodic oxidation process.²⁷ This weight loss disappeared, however, upon calcination of the plate at 500 °C in nitrogen, as can be seen in the anatase Ti/C-TNTAs thermogram. The APTESfunctionalized sample, anatase Ti/C-TNTAs-NH₂(0.8%), displays a 0.63% weight loss at 600 °C that indicates the presence of the aminotrimethyl silane functionality on the TiO₂ nanotubes. Meanwhile, the anatase Ti/C-TNTAs-NH₂(0.8%)@HEP electrode shows 1.21% weight loss upon

heating to $600\,^{\circ}\text{C}$ because of the presence of adsorbed HEP molecules onto the plate surface.

The morphological features of the Ti/C-TNTAs and Ti/ C-TNTAs-NH₂ were identified using scanning electron microscopy (SEM). Top-view and cross-sectional SEM images of the anatase Ti/C-TNTAs and anatase Ti/C-TNTAs-NH₂ substrates at different magnifications are shown in Figure 2a,b. The SEM micrographs reveal the well-ordered nanotubes on the Ti support. The SEM images of the anatase Ti/C-TNTAs-NH₂ material also suggest the APTES film is wellformed on the wall of the nanotubes. Moreover, the tube pores remain open after APTES functionalization, indicating the porous structure is well-maintained, which is crucial for the electrochemical performance and adsorption efficiency of anatase Ti/C-TNTAs-NH₂.32 The average width of the nanotube openings was ~70 nm, with a wall thickness of around 10 nm. Cross-sectional SEM images of the anatase Ti/ C-TNTAs and anatase Ti/C-TNTAS-NH2 samples reveal the TNTAs are around 2 μ m in length (Figure 2a,b).

We utilized energy dispersive X-ray (EDX) elemental mapping to analyze the elemental content of the anatase Ti/C-TNTAs-NH₂ substrate. The results clearly indicate that Ti, C, O, F, Si, and N elements are present in the anatase Ti/C-TNTAs-NH₂ (Figure 2c). The EDX maps for Si and N elements show that the APTES film is well-distributed around the tube's opening. We assume the observed fluoride ions originate from the anodic oxidation in ethylene glycol/ammonium fluoride, which can cause TiF₄, TiOF₂, and pentafluoro-aquo-titanate to form and cause the incorporation of fluoride ions into the TNTAs. All of these results combined indicate the anatase TNTAs structure was successfully grown onto the Ti substrate and that APTES had been successfully attached as a thin layer onto the surface of TNTAs.

The formation of APTES film onto TNTAs was further examined by atomic force microscope (AFM). Figure S2 shows the AFM topographic images ($10.0~\mu \times 10.0~\mu$) of the anatase Ti/C-TNTAs, anatase Ti/C-TNTAs-NH₂(0.8%), and anatase Ti/C-TNTAs-NH₂(1.2%), and Table 1 lists the

Table 1. Surface Roughness of Anatase Ti/C-TNTAs Compared with Two Modified Samples Using Different APTES Loadings^a

sample	roughness average (Ra) (nm)	root-mean-square roughness (Rq) (nm)
anatase Ti/C-TNTAs	83.16	105.44
anatase Ti/C-TNTAs- NH ₂ (0.8%)	75.19	92.63
anatase Ti/C-TNTAs-NH ₂ (1.2%)	67.39	83.21

^aAnatase Ti/C-TNTAs-NH₂ (0.8% and 1.2%).

roughness average (Ra) and root-mean-square roughness (Rq) values of these samples. The anatase Ti/C-TNTAs sample shows a very high average roughness of 83.16 nm. However, the roughness of the material dramatically decreases after APTES modification (Figure S2 and Table 1). The roughness for both modified TNTs (anatase Ti/C-TNTAs-NH₂(0.8% and 1.2%)) is close together while the sample with a higher loading of APTES (1.2%) shows a lower roughness, due to higher functionalization, which is also confirmed by the

magnified AFM topographic images (2.0 μ × 2.0 μ) in Figure S3.

We measured the water contact angles of the fabricated electrodes to determine their hydrophilicity, which is an important characteristic property affecting the adsorption efficiency of support. Figure S4 shows the water contact angles (Θ_{w}) of the Ti foil compared to the anatase Ti/C-TNTAs plate before and after APTES functionalization. The $\Theta_{\rm w}$ of the Ti foil is 70.4°, while after the growth of the TiO₂ nanotubes via anodic oxidation Θ_w increased to 103.4°. However, after modification with APTES, the $\Theta_{\rm w}$ of the Ti/C-TNTAs-NH₂ plate decreased from 87.4° to 8.4° as the amount of APTES increased from 0.4% to 1.2%. We ascribe the improvement of the hydrophilic properties to the wettability of the APTES film on the hydrophobic TNTAs surface. This progressive decrease in Θ_w indicates the successful functionalization of Ti/C-TNTAs with APTES at different concentrations.

To fabricate the cathode (Scheme 1b), we formed expanded graphite (a porous version of the material) by exposing the graphite to $\rm H_2SO_4/HNO_3$, followed by thermal shock at 900 °C for 1 min (see Supporting Information). The expanded graphite was selected because of its high capacity in adsorption of proteins as probable interfering species in the reaction mixture of HEP. SEM images of graphite and expanded graphite are shown in Figure S5. The expanded graphite forms when the material is quickly heated at a high temperature due to the evaporation of the incorporated $\rm H_2SO_4/HNO_3$, causing the graphite sheets to enlarge along the symmetry axis (C-axis), becoming expanded sheets. The expansion volume of expanded graphite after the exfoliation process (acidic treatment followed by a thermal shock at 900 °C) was ~200 mL $\rm g^{-1}$, which is about 1000 times larger than the parent graphite material.

Electrosorption. Electrosorption experiments were performed at 25 °C in a three-electrode setup using the anatase $Ti/C-TNTAs-NH_2(0.8\%)$ plate as the anode, the expanded graphite as the cathode, and a saturated calomel electrode (SCE, +0.24 V) as the reference electrode. The electrolyte contained 25 mL of aqueous HEP solution (50 mg L⁻¹) and 0.1 M NaClO₄. NaClO₄ was selected as the background electrolyte because it does not undergo specific adsorption and therefore will not interact with the adsorption behavior of the examined species.³⁷ We began the electrosorption process by applying a constant potential of +1000 mV to the Ti/C-TNTAs-NH₂ vs SCE under continuous stirring, presumably causing some of the negatively charged HEP to adsorb to the Ti/C-TNTAs-NH2 surface. To determine the amount of HEP that remained in solution, we utilized a methylene blueassisted spectrophotometric technique described in detail in our previous publication.5 The HEP electrosorption performance of the Ti/C-TNTAs-NH2 plate was assessed at different conditions, including both with/without applying a potential, using different ratios of APTES modification, and comparing with the performance of Ti and Ti/C-TNTAs plates (Figure 3a). According to our results, the Ti and Ti/C-TNTAs plates did not demonstrate any ability of HEP adsorption, not even after applying an external potential to the cell. We hypothesize that this behavior occurs due to the absence of potential binding sites onto the adsorbate. Interestingly, the situation was completely changed when the Ti/C-TNTAs plate was modified by 0.4% APTES (Figure 3a), likely due to the terminal NH₂ groups providing a high density of positive

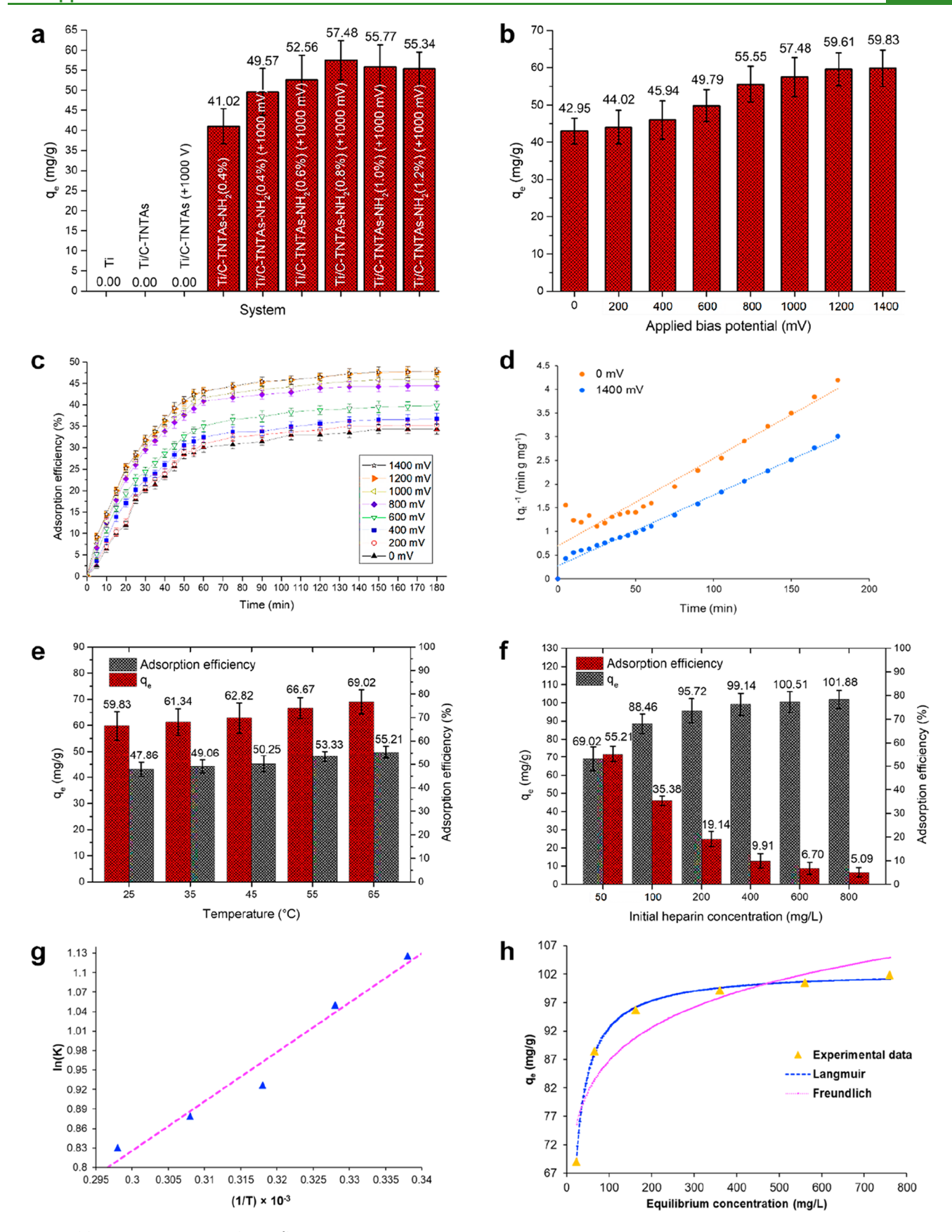


Figure 3. (a) Adsorption capacity (mg g $^{-1}$) of various systems, including Ti, Ti/C-TNTAs, and Ti/C-TNTAs-NH $_2$ with different loadings of APTES (0.4%, 0.6%, 0.8%, 1.0, and 1.2%), both with or without +1000 mV potential in the recovery of pure HEP (50 mg L $^{-1}$) (temperature 25 °C, pH 7, and reaction time 3 h). (b) Adsorption capacity (mg g $^{-1}$) and (c) adsorption efficiency of Ti/C-TNTAs-NH $_2$ (0.8%) toward HEP (50 mg L $^{-1}$) as a function of applied potential (temperature of 25 °C, pH of 7, and reaction time of 3 h). (d) The pseudo-second-order kinetic plot for the electrosorption of HEP onto Ti/C-TNTAs-NH $_2$ (0.8%). The adsorption capacity (mg g $^{-1}$) and adsorption efficiency of Ti/C-TNTAs-

Figure 3. continued

 $NH_2(0.8\%)$ toward HEP as a function of (e) temperature (applied potential of +1400 mV, initial HEP concentration of 50 mg L⁻¹, pH of 7, and reaction time of 3 h) and (f) initial HEP concentration (applied potential of +1400 mV, temperature of 65 °C, pH of 7, and reaction time of 3 h). (g) The plots of ln(K) vs 1/T and (h) adsorption isotherms for the electrosorption of HEP onto Ti/C-TNTAs- $NH_2(0.8\%)$.

Table 2. Thermodynamic Parameters for the Electrosorption of HEP onto the $Ti/C-TNTAs-NH_2(0.8\%)$ as a Function of Temperature

			$-\Delta G^{\circ}$ (kJ mol ⁻¹)				
contact time (h)	$-\Delta H^{\circ}$ (J mol ⁻¹)	$-\Delta S^{\circ}$ (J (mol K) ⁻¹)	298	308	318	328	338
5	63.25	12.11	3.546	3.667	3.789	3.910	4.031

charges that serve as binding sites to form strong electrostatic interactions with the HEP molecules in solution. The NH₂ groups have a p K_a of \sim 9; so, they protonate at pH < 9 and lead to the formation of NH₃⁺ groups. Applying an external potential further improved the adsorption capacity (i.e., the amount of HEP adsorbed) of the Ti/C-TNTAs-NH₂(0.4%) anode toward HEP. By applying an external potential (+1000 mV vs SCE), making the anodic Ti/C-TNTAs-NH₂(0.4%) plate more positively charged, the HEP adsorption capacity increased from 42.95 to 51.49 mg g⁻¹. Clearly, the external potential plays an important role in driving anionic HEP molecules onto the positively charged Ti/C-TNTAs-NH₂(0.4%) plate.

We also examined the effect of the APTES concentration used to functionalize the anode surface in terms of the electrode's HEP electrosorption capability. In order to achieve an NH2-functionalized Ti/C-TNTAs plate with different loadings of amino groups, we added different concentrations of APTES (0.4, 0.6, 0.8, 1, and 1.2% v/v) to the solution during postmodification of the Ti/C-TNTAs plate. The Ti/C-TNTAs-NH₂ plate with 0.8% v/v showed a high adsorption capacity of 59.40 mg g⁻¹ at +1000 mV potential. However, further increasing the initial concentration of APTES did not have a positive effect on the electrosorption efficiency of the Ti/C-TNTAs-NH₂. For example, the Ti/C-TNTAs-NH₂ plate with 1.2% v/v showed an adsorption capacity of 52.99 mg g⁻¹ at +1000 mV potential. Apparently, there is a threshold APTES concentration for Ti/C-TNTAs surface modification, after which further functionalization is not possible, as the electrosorption efficiency of the samples made with 0.8% APTES and higher showed similar values within the experimental error (Figure 3a). In addition, a high concentration of silane coupling agent can form a thick layer of APTES onto the Ti/C-TNTAs electrode, blocking the mouth and openings of the TNTs, reducing the surface area of the electrode and its electrochemical performance. Based on the electrosorption efficiency results, the Ti/C-TNTAs-NH₂(0.8%) anode demonstrating the highest electrosorption capacity toward HEP was chosen for subsequent analysis.

The FTIR spectra of the $Ti/C-TNTAs-NH_2(0.8\%)$ anode before and after electrosorption of HEP (Figure S6) revealed that the intensity of most of the absorption bands reduced after HEP sorption, which suggests the successful electrosorption of HEP molecules onto the $Ti/C-TNTAs-NH_2(0.8\%)$ anode. The EDX map for elemental S in the anatase $Ti/C-TNTAs-NH_2(0.8\%)$ after HEP electrosorption process (Figure S7) also clearly confirms that HEP had been successfully attached onto the surface of the TNTAs.

We studied the effect of the applied bias potential (0, +400, +600, +800, +1000, +1200, and +1400 mV vs SCE) on the

electrosorption efficiency of the Ti/C-TNTAs-NH₂ system. We observed the adsorption capacity to increase along with the potential (Figure 3b), in which an adsorption capacity of 59.83 mg g⁻¹ was achieved for an electrochemical polarization of +1400 mV, while it was 42.95 mg g⁻¹ at the same set of conditions but without bias. Figure 3c shows the adsorption efficiency of HEP onto the Ti/C-TNTAs-NH₂ plate as a function of the applied potential over time. Like the adsorption capacity, the adsorption efficiency of HEP increased as the applied bias potential increased from 0 to +1400 mV. Compared to the system without potential, the adsorption efficiency increased by 28.22% with an electrochemical polarization of +1400 mV. Consequently, we deduced that applying an external potential significantly increased the adsorption efficiency and capacity of the Ti/C-TNTAs- $NH_2(0.8\%)$ toward HEP. To avoid the electrolysis of water, we were limited in applying potentials lower than +1800 mV.³⁸ The obtained adsorption kinetic results (shown in Figure 3c) were evaluated by fitting using a pseudo-second-order kinetic model (Table S1). The adsorption rate constant, k_2 , for 0 and +1400 mV were found to be 4.8×10^{-4} and 8.2×10^{-4} g mg⁻¹ min⁻¹, respectively, indicating the rapid capture of HEP from aqueous solutions at +1400 mV (Figure 3d). This implies that the adsorption process through the porous material may be limited by intraparticle diffusion.³⁹ In fact, the fast adsorption rate may be related to the porous framework of the nanotubes, as well as the distribution of the high density of NH₂ groups on the $Ti/C-TNTAs-NH_2(0.8\%)$ plate, in which the available adsorption sites increase by applying the external potential.

We also studied the effects of solution temperature and initial HEP concentration on the electrosorption efficiency of the $Ti/C-TNTAs-NH_2(0.8\%)$ plate (Figure 3e,f). The adsorption efficiency of HEP increased from 47.86% to 55.21% by increasing the solution temperature from 25 to 65 °C. The adsorption capacity also followed a similar trend, rising from 59.83 to 69.02 mg g⁻¹ as the solution temperature increased from 25 to 65 °C, suggesting the adsorption process is endothermic. This behavior may be related to the increased diffusion of the HEP molecules across the exterior boundary layer and into the interior pores of the nanotubes due to the reduced viscosity of the solution with increasing temperature. 40,41 We evaluated the effect of elevated temperature on the Gibbs free energy (ΔG) , the enthalpy change (ΔH) , and the entropy change (ΔS) of HEP electrosorption onto the Ti/ C-TNTAs-NH₂(0.8%), in which the ΔG values for the HEP electrosorption were obtained by the following equations: 42 $\Delta G = -RT \ln K$ and $\ln K = \Delta S^{\circ}/R - \Delta H^{\circ}/RT$. The ΔH° and ΔS° values were plotted from the slope and intercept of the linear plot of $\ln K$ vs 1/T (Figure 3g and Table 2). For all of the temperatures studied, the value of ΔG was negative, which

implies the electrosorption process onto Ti/C–TNTAs–NH₂(0.8%) is spontaneous and thermodynamically favorable. Both the ΔH° and ΔS° values were negative, which confirmed that capture of HEP on the surface of the Ti/C–TNTAs–NH₂(0.8%) anode involves the release of some energy during the interaction between the opposite charges and decreasing the energy freedom and order of the electrochemical system after capture of the HEP. 43,44

A different behavior was observed in studying the effect of the initial HEP concentration (Figure 3f). The adsorption efficiency decreased from 55.21% to 5.09% by increasing the initial HEP concentration from 50 to 800 mg L⁻¹. We hypothesize this trend was observed because of the limited number of NH₂ active groups on the Ti/C-TNTAs-NH₂(0.8%) plate, which can become completely saturated when the HEP concentration is high enough. 45 Interestingly, the amount of HEP adsorbed onto the Ti/C-TNTAs- $NH_2(0.8\%)$ plate increased from 69.02 mg g⁻¹ to 101.88 mg g⁻¹ as the concentration of HEP was increased. We attributed this to the driving force generated by a high concentration of HEP molecules, which overcome the mass transfer resistance of HEP from the solution to the surface of the Ti/C-TNTAs-NH₂(0.8%) plate. 46 We fitted the experimental isotherm data to the Langmuir and Freundlich models to better understand the HEP capture mechanism by the Ti/C-TNTAs-NH₂(0.8%) plate (see Table S1). The Langmuir model implies that electrosorption could be performed through one layer of adsorbate on the active site of the adsorbent, 47 while the Freundlich model suggests that active sites of the adsorbent are heterogeneous and the adsorption process occurs through multilayers of adsorbate. 48 Based on the results shown in Table 3 and Figure 3h, we found that

Table 3. Parameter Fittings of the Equilibrium Isotherm Results for Different Initial Concentrations of HEP to the Langmuir and Freundlich Equation Parameters

isotherm models	$q_{ m m}$	$K_{ m L}$	K_{F}	n	R^2
Langmuir	102.6	9.23×10^{-2}			0.9983
Freundlich			56.4	1	0.864

electrosorption process onto $Ti/C-TNTAs-NH_2(0.8\%)$ obeyed the Langmuir isotherm model ($R^2=0.9983$), suggesting the electrosorption of HEP on the active site of the immobilized APTES occurs in a monolayer.

Mechanism of HEP Electrosorption. We used X-ray photoelectron spectroscopy (XPS) to study the chemical surfaces and interactions of HEP with the active sites of the Ti/C-TNTAs-NH₂ plate. Figure 4a-k shows the XPS spectra of the Ti/C-TNTAs, Ti/C-TNTAs-NH2, and Ti/ C-TNTAs-NH₂@HEP substrates. After modification of Ti/ C-TNTAs with APTES, Si and N signals appeared in the Ti/ C-TNTAs-NH₂ sample, which further confirmed successful functionalization of the Ti/C-TNTAs (Figure 4a). Meanwhile, adsorbing HEP onto the surface of the Ti/C-TNTAs-NH₂ resulted in a new peak (S 2p) related to the sulfonate groups of the HEP. The O 1s, C 1s, and N 1s spectra of the Ti/C-TNTAs, Ti/C-TNTAs-NH₂, and Ti/C-TNTAs-NH₂@HEP samples are shown in Figure 4c-j. In Figure 4b, Ti 2p doublet peaks of Ti/C-TNTAs with both Ti 2p 1/2 and Ti 2p 3/2 (Ti³⁺) components appeared at 465.0 and 459.4 eV. However, a binding energy of 461.6 eV was also observed, which could be related to the Ti 2p 3/2 orbital (Ti⁴⁺). 49,50 The

O 1s spectrum of Ti/C-TNTAs (Figure 4c) showed two peaks at 530.5 and 532.5 eV, which are related to oxygen atoms in the lattice structure of the TNTs and hydroxyl groups on the surface of the TNTs, respectively. 51 The O 1s region of Ti/C-TNTAs-NH₂ is shown in Figure 4d, in which all of the peaks related to the oxygen of the TiO2 shifted to higher binding energies compared to Ti/C-TNTAs, which implies that the surface of the Ti/C-TNTAs was successfully treated with silane groups of the APTES, additionally resulting in a broad peak at 536.1 eV related to the adsorbed water on the amine groups. 52 By adsorbing the HEP onto the surface of the Ti/C-TNTAs-NH₂, the peak at 536.1 eV disappears, confirming that the amine groups of the APTES are involved in the interaction with HEP and desorbed water molecules (Figure 4e). Figure 4f—h shows the deconvolution of the C 1s spectra of Ti/C-TNTAs, Ti/C-TNTAs-NH₂, and Ti/C-TNTAs-NH₂@HEP, respectively. The peak at 285.5 eV may be related to the C=C and C-C bonds of the remaining calcined carbon in the framework of the TNTAs. However, peaks after 290 eV are attributed to C—O—C and O—C=O (Figure 4f-h).⁵³ The N 1s spectra of Ti/C-TNTAs-NH₂ showed a peak at 403.9 eV, which belongs to the amine groups of the immobilized APTES on the surface of the TNTs (Figure 4i). After adsorption of HEP onto the surface of Ti/C-TNTAs-NH₂, the amine peak shifted to a lower binding energy (401.5 eV, Figure 4j) and a new peak related to the S 2p spectrum of the sulfonate group of HEP appeared at 170.4 eV (Figure 4k). In fact, the negative binding energy shift (\sim 2 eV) of the N 1s spectra of the Ti/C-TNTAs-NH2@HEP could be attributed to the formation of a negative space charge layer of HEP molecules on the surface of the Ti/C-TNTAs- NH_{2}^{54}

Regeneration and Reusability of Ti/C-TNTAs-NH₂. As HEP must eventually be extracted and commercial HEP adsorbents are typically reused to lower their costs, we studied the ability of the Ti/C-TNTAs-NH2@HEP plate to desorb and release HEP using an aqueous solution of NaCl and applying an external potential. We hypothesized that the replacement of HEP molecules adsorbed onto the Ti/C-TNTAs-NH₂ electrode could be achieved with Cl⁻ ions present in the aqueous solution (Scheme 1c). Electrodesorption experiments were carried out in the same setup as used in the HEP electrosorption test. In each run, 25 mL of a NaCl aqueous solution with different initial concentrations (2.5%, 5%, 10%, 20%, and 35%) was added into the cell. The electrodesorption process was begun by applying a constant anodic or cathodic potential (-600, -400, -200, 0, +200,+400, +600, +800, +1000, +1200, and +1400 mV) to the Ti/ C-TNTAs-NH2@HEP vs SCE under continuous stirring for 1 h. Figure 5a shows the effect of the bias potential applied to the Ti/C-TNTAs-NH₂@HEP electrode on the desorption efficiency of HEP in a 5% NaCl solution. The desorption efficiency was defined as the ratio of the desorbed amount of HEP from the surface of Ti/C-TNTAs-NH₂ to the initial adsorbed amount of HEP. We observed that applying a cathodic potential to the Ti/C-TNTAs-NH2@HEP plate had a negative effect on the desorption of HEP. The desorption efficiencies were 1.4%, 4.95%, and 5.57%, when the applied cathodic potentials were -600, -400, and -200mV. As can be seen, the desorption efficiency decreased with an increasing cathodic bias potential. When no potential was applied, the desorption efficiency of HEP from the surface of the Ti/C-TNTAs-NH₂@HEP plate in the presence of 5%

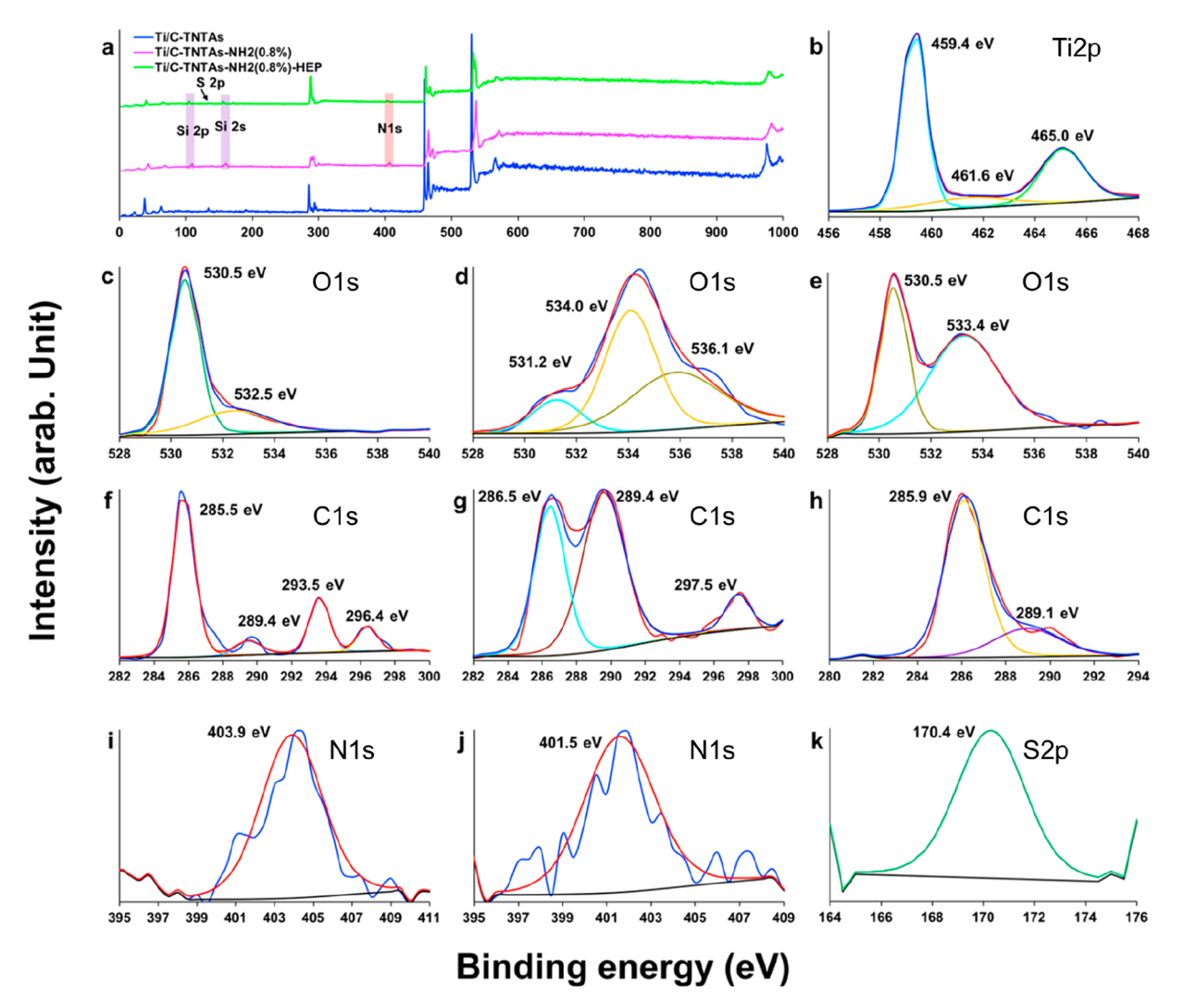


Figure 4. (a) XPS survey scans for Ti/C-TNTAs, Ti/C-TNTAs-NH₂, and Ti/C-TNTAs-NH₂@HEP. High-resolution scans of the Ti 2p, O 1s, C 1s, N 1s, and S 2p spectra (b, c, f) for Ti/C-TNTA (d, g, i), Ti/C-TNTAs-NH₂ (e, h, j, k), and Ti/C-TNTAs-NH₂@HEP.

NaCl was greater than when a cathodic potential was used. A desorption efficiency of 16.10% was obtained from using just 5% NaCl without a potential. However, by applying an anodic potential to the Ti/C-TNTAs-NH₂@HEP plate in the presence of 5% NaCl, the desorption efficiency of HEP improved and increased along with the anodic potential to a maximum value of 25.39% at +1400 mV. These results show that the desorption efficiency of HEP from the surface of the Ti/C-TNTAs-NH₂@HEP plate in the anode mode was higher than that in the cathode mode. We believe that when the anode has a positive charge on its surface, this enables the electrosorption of Cl⁻ ions, which replace HEP molecules, allowing the HEP to easily desorb and release into solution from the anodic Ti/C-TNTAs-NH₂@HEP plate.

We studied the effect of the initial concentration of NaCl in the anodic mode of regenerating the ${\rm Ti/C-TNTAs-NH_2@MEP}$ electrode. Figure 5b shows the effect of the NaCl concentration on the regeneration efficiency of the electrochemical cell toward HEP adsorption when an anodic potential (+1400 mV) was applied to the ${\rm Ti/C-TNTAs-NH_2@HEP}$ plate, and the results of which are compared with the nonpotential applied mode. At a NaCl concentration of 10%, the regeneration efficiency of the anodic ${\rm Ti/C-TNTAs-}$

NH₂@HEP plate with +1400 mV potential was 54.49%, while at the same conditions for the non-potential mode the regeneration efficiency was 22.29%. At a NaCl concentration of 15%, the regeneration efficiencies of the anodic Ti/C-TNTAs-NH₂@HEP plate with +1400 mV and 0 mV applied potential were 68.42% and 32.20%, respectively. Finally, extremely high regeneration efficiencies of 92.56% and 89.78% were obtained for the anodic Ti/C-TNTAs-NH₂@HEP plate at +1400 mV and 0 mV applied potential in the presence of saturated NaCl (36%). These results demonstrate that the regeneration of the adsorbent can be improved by applying an anodic potential to the plate, as well as by increasing the concentration of NaCl in solution.

The reusability of HEP adsorbents is an important factor for industrial applications. Therefore, we studied the reusability of the anodic ${\rm Ti/C-TNTAs-NH_2}$ plate toward HEP electrosorption after ten electrosorption/electrodesorption cycles in the presence of saturated NaCl (36%) at an applied anodic potential of +1400 mV. Figure 5c shows the adsorption capacity of ${\rm Ti/C-TNTAs-NH_2}(0.8\%)$ toward HEP as a function of the number of regeneration cycles. The adsorption capacity of ${\rm Ti/C-TNTAs-NH_2}(0.8\%)$ dropped to 65.75 mg g⁻¹ from 69.02 mg g⁻¹, after the first regeneration and reuse,

ACS Applied Bio Materials Article

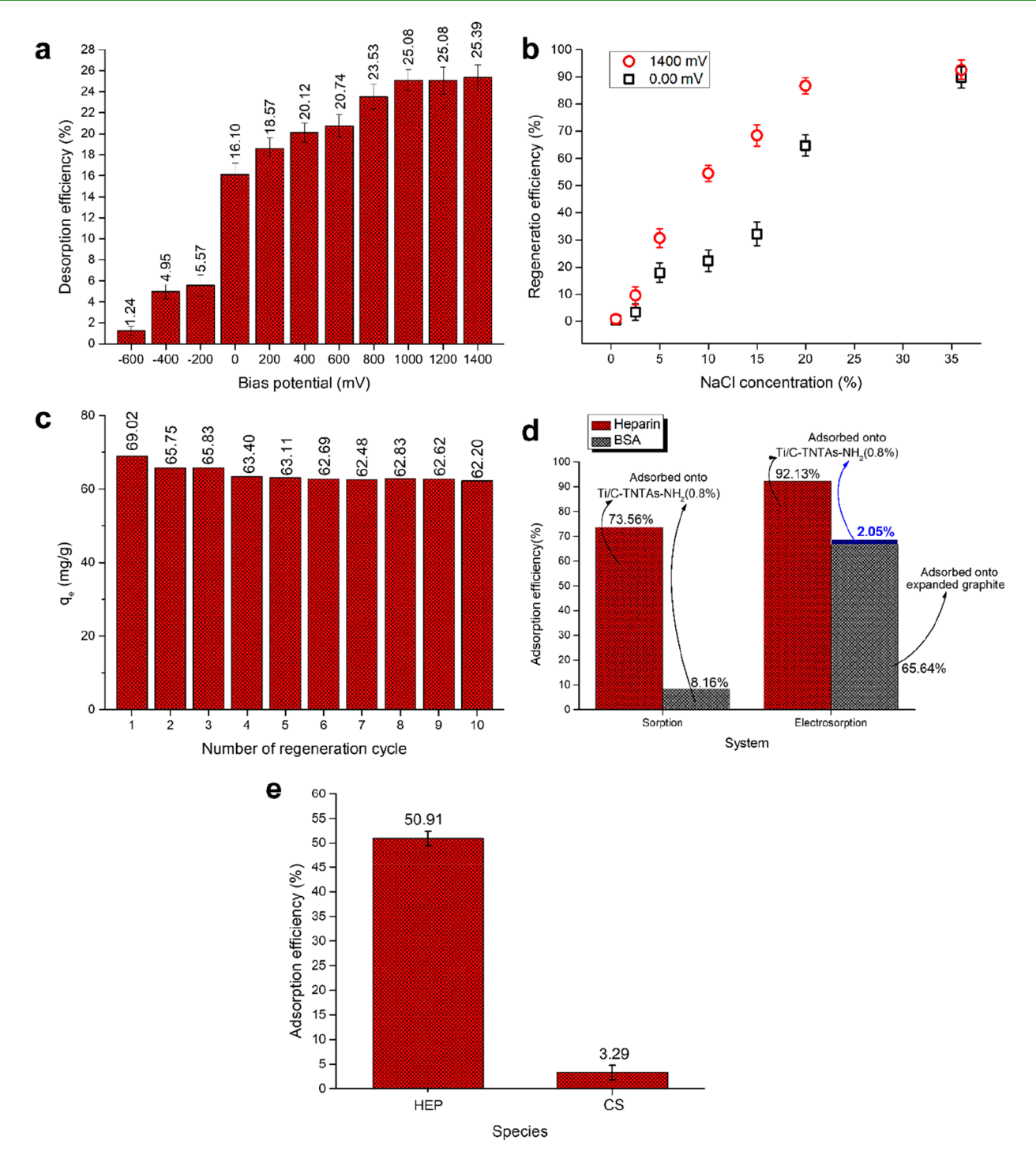


Figure 5. (a) HEP desorption efficiency (%) of $Ti/C-TNTAs-NH_2@HEP$ as a function of the applied bias potential (NaCl concentration of 5%, temperature of 55 °C, reaction time of 1 h). (b) Regeneration efficiency (%) of $Ti/C-TNTAs-NH_2@HEP$ as a function of NaCl concentration (applied bias potential of +1400 mV, temperature of 65 °C, initial HEP concentration of 50 mg L^{-1} , pH of 7, reaction time of 3 h). (c) Adsorption capacity (mg g $^{-1}$) and reusability of $Ti/C-TNTAs-NH_2(0.8\%)$ toward HEP (50 mg L^{-1}) as a function of regeneration cycles (applied bias potential of +1400 mV, temperature of 65 °C, initial HEP concentration of 50 mg L^{-1} , pH of 7, and reaction time of 3 h). (d) Adsorption efficiency and selectivity of $Ti/C-TNTAs-NH_2$ toward HEP in a mixture of HEP/BSA using different systems, including regular sorption ($Ti/C-TNTAs-NH_2$ without applying a potential) and electrosorption (anodic $Ti/C-TNTAs-NH_2$ /cathodic expanded graphite with an applied potential of +1400 mV) (temperature of 65 °C, initial HEP concentration of 25 mg L^{-1} , initial BSA concentration of 25 mg L^{-1} , pH of 4, and reaction time of 3 h). (e) Specificity of the designed electrochemical system toward HEP in a mixture of HEP/CS (applied bias potential of +1400 mV, temperature of 65 °C, initial HEP concentration of 50 mg L^{-1} , initial CS concentration of 10 mg L^{-1} , pH of 7, and reaction time of 3 h).

eventually reaching 62.20 mg g⁻¹ after ten regeneration/reuse cycles, which amounts to maintaining 90.11% of its initial efficiency toward HEP electrosorption after ten cycles of reuse,

indicating the stability of the system. In addition, after several usages of the ${\rm Ti/C-TNTAs-NH_2}$ plate, it is possible to thoroughly clean its surface and prepare it for refunctionaliza-

tion by annealing at a high temperature or using an ultra-violet light, due to the excellent photocatalytic behavior of the anatase TNTs.55-57

Selectivity of Ti/C-TNTAs-NH₂ toward HEP. Our main purpose in designing this electrochemical system was to apply it for the selective capture of HEP in the presence of a variety of species available in a HEP digestion mixture from natural tissue, including proteins, nucleic acids, etc. Because of this, we used a synthetic mixture of HEP and BSA protein at the same concentrations (25 mg L⁻¹) as a model compound to simulate a complex biological material to evaluate the selectivity of the Ti/C-TNTAs-NH₂ plate. An HPLC-DAD system equipped with a Dionex IonPac AS11-HC column (2 mm × 250 mm) and operated at a flow rate of 0.2 mL min⁻¹ was used to evaluate the concentration of each component in the mixture. Final samples were run using an HPLC-DAD system to evaluate the concentration of each component. In an innovative idea, this time, the expanded form of a graphite plate was used as a cathode, instead of the platinum plate. The high capacity of expanded graphite in adsorption of proteins such as BSA is well-known and frequently reported in the literature. 35,36 The setup and specificity of the designed electrochemical system toward HEP in a mixture of HEP/ BSA are illustrated in Scheme 1d. Figure 5d shows the adsorption efficiency and selectivity of HEP and BSA in a mixture using different systems, including regular sorption (Ti/ C-TNTAs-NH₂ without applying a potential) and electrosorption (anodic Ti/C-TNTAs-NH₂/cathodic expanded graphite with an applied +1400 mV potential). In the sorption mode using only the Ti/C-TNTAs-NH₂ plate and without applying a potential, 73.56% of the HEP and 8.16% of the BSA were adsorbed onto the plate. However, in electrosorption mode with the Ti/C-TNTAs-NH2 plate as the anode and expanded graphite as the cathode at a potential of +1400 mV, 92.13% of the HEP and 2.05% of the BSA were adsorbed onto the anodic Ti/C-TNTAs-NH₂, while 65.64% of the BSA was adsorbed onto the cathodic expanded graphite. These results clearly indicate the superiority of the electrosorption system compared to traditional sorption in the selective separation of HEP in the presence of protein molecules like BSA. We believe the applied +1400 mV of potential makes the Ti/C-TNTAs-NH₂ anode more positively charged and therefore better able to adsorb negatively charged HEP molecules with an average ζ potential of -4.9 mV at pH 4. Meanwhile, the expanded graphite cathode is negatively charged under these conditions, which enables it to adsorb the positively charged BSA molecules with an average ζ potential of +7.1 mV at pH 4. It should be noted that the pH of the HEP/BSA mixture for the selectivity test was adjusted to 4, since at this pH the HEP and BSA feature opposite charges.

Additionally, we investigated the specificity of our electrochemical system by studying other kinds of probable interfering species, such as CS, which is a negatively charged sulfated glycosaminoglycan with a similar structure as HEP (Figure 5e). A synthetic mixture of 50 mg L^{-1} HEP and 10 mg L⁻¹ CS was prepared, and a low concentration of CS was selected because it acts as an interfering species. We observed that our setup had a very low adsorption efficiency (3.29%) toward CS. However, the adsorption efficiency for HEP was just 50.91%. These results indicate the good sorption specificity of the Ti/C-TNTAs-NH2 anode for HEP molecules.

Real Sample Test. To demonstrate the actual performance of our system, we evaluated its performance using a real sample composed of a biological mixture containing HEP (50 mg L^{-1}) enzymatically isolated from porcine intestinal mucosa. The initial and residual HEP concentration in the real sample before and after electrosorption experiments was measured using a HEP-ELISA kit (MyBiosource, San Diego, CA, USA). An adsorption efficiency of 43.25% and capacity of 54.06 mg g⁻¹ were achieved using the anodic Ti/C-TNTAs-NH₂ and cathodic expanded graphite when the applied potential was +1400 mV, the solution temperature was 65 °C, and the pH of solution was 7. We further evaluated the performance of the electrochemical system at different initial concentrations of the real sample, prepared by dilution of the 50 mg L⁻¹ stock solution (Figure S8). The same trend was observed in the case of the real samples at different initial concentrations, in which the adsorption efficiency increased from 43.25% to about 100% by dilution of the 50 mg L^{-1} real sample to 10 mg L^{-1} . However, the adsorption capacity decreased from 54.06 mg $\rm g^{-1}$ to 24.75 mg g⁻¹ as the concentration of the real sample was diluted to 10 mg L⁻¹.

We also measured the anticoagulant potency of the HEP desorbed from the surface of the Ti/C-TNTAs-NH@HEP plate in the real sample test using a sheep plasma clotting assay described in detail elsewhere. 11,58 The ability of HEP desorbed from the surface of the Ti/C-TNTAs-NH plate to prevent the clotting of citrated sheep plasma was compared with that of a HEP sodium reference standard, which was calibrated by United States Pharmacopeia. The semiclotting point for HEP electrodesorbed from the surface of the Ti/C-TNTAs-NH@ HEP plate was found to be 95 μ L. The final recovered HEP product had an anticoagulant potency of 2.93 U mL⁻¹ and a total bioactivity 2347 units, which fulfills the prerequisites of the United States Pharmacopeia (see eq S1 in the Supporting Information for calculations).

CONCLUSION

Herein, we have demonstrated an electrochemical system composed of anodic Ti/C-TNTAs-NH2 and cathodic expanded graphite, which we employed to electrochemically capture and release HEP digested from porcine intestinal mucosa, enabling it for further purification. Applying an external potential played an important role in driving the anionic HEP molecules onto the positively charged anodic Ti/ C-TNTAs-NH₂ plate and improved the HEP adsorption capacity from 42.95 mg g⁻¹ to 51.49 mg g⁻¹. The HEP electrosorption efficiency improved with an increasing applied bias potential (0 to +1400 mV vs SCE) and solution temperature (25-65 °C); however, there was an optimal concentration (0.8%) for APTES. Applying a cathodic potential (-600 to -200 mV vs SCE) to the Ti/C-TNTAs-NH₂@HEP plate had a negative effect on the regeneration of the plate and desorption of HEP from its surface. The desorption of HEP from the plate surface can be improved by applying an anodic potential to the plate (+200 to +1400 mV vs SCE), as well as by increasing the concentration of NaCl (2.5-36%) in solution. We characterized the anodic Ti/C-TNTAs-NH2 and cathodic expanded graphite electrodes using various techniques, including XRD, FTIR, TGA, SEM, EDX, AFM, XPS, and water contact angle. XPS analysis confirmed that the amine functional groups on the nanotube surfaces are highly inclined toward the sulfonate groups of HEP because of strong electrostatic interactions. We evaluated

the productivity and selectivity of this electrochemical cell for HEP in a simulated mixture of probable interfering species, such as CS and BSA, as well as in a real sample composed of a biological mixture including HEP enzymatically digested from porcine intestinal mucosa. Our results demonstrate that this electrochemical system has a very low adsorption efficiency toward such probable interfering species (2.05% toward BSA and 3.29% toward CS) and clearly demonstrates the strong electrosorption specificity of HEP molecules.

ASSOCIATED CONTENT

S Supporting Information

The Supporting Information is available free of charge on the ACS Publications website at DOI: 10.1021/acsabm.9b00400.

Materials and methods, optical photos, AFM topographic images, water contact angles, SEM images, FTIR spectra, EDX map, adsorption capacity and adsorption efficiency, normalized electrosorption data, electrosorption isotherm, and kinetics equations (PDF)

AUTHOR INFORMATION

Corresponding Author

*E-mail: alireza@cornell.edu. Tel: (607) 255-2923.

ORCID (

Hamed Eskandarloo: 0000-0001-7241-119X Mojtaba Enayati: 0000-0002-4408-2808 Alireza Abbaspourrad: 0000-0001-5617-9220

Notes

The authors declare no competing financial interest.

ACKNOWLEDGMENTS

This work made use of the Cornell Center for Materials Research's Shared Facilities, which are supported through the NSF MRSEC program (DMR-1719875). This publication was made possible by research funding provided by the Shineway Company (WH Group, China).

REFERENCES

- (1) Lee, J.-C.; Lu, X.-A.; Kulkarni, S. S.; Wen, Y.-S.; Hung, S.-C. Synthesis of Heparin Oligosaccharides. *J. Am. Chem. Soc.* **2004**, *126* (2), 476–477.
- (2) Lever, R.; Mulloy, B.; Page, C. P. Heparin A Century of Progress; Springer Berlin Heidelberg, 2012.
- (3) Xiao, Z.; Tappen, B. R.; Ly, M.; Zhao, W.; Canova, L. P.; Guan, H.; Linhardt, R. J. Heparin Mapping Using Heparin Lyases and the Generation of a Novel Low Molecular Weight Heparin. *J. Med. Chem.* **2011**, *54* (2), 603–610.
- (4) van der Meer, J.-Y.; Kellenbach, E.; van den Bos, J. L. From Farm to Pharma: An Overview of Industrial Heparin Manufacturing Methods. *Molecules* **2017**, 22 (6), 1025.
- (5) Eskandarloo, H.; Godec, M.; Arshadi, M.; Padilla-Zakour, O. I.; Abbaspourrad, A. Multi-porous quaternized chitosan/polystyrene microbeads for scalable, efficient heparin recovery. *Chem. Eng. J.* **2018**, 348, 399–408.
- (6) Kamiński, K.; Zazakowny, K.; Szczubiałka, K.; Nowakowska, M. pH-Sensitive Genipin-Cross-Linked Chitosan Microspheres For Heparin Removal. *Biomacromolecules* **2008**, 9 (11), 3127–3132.
- (7) Wei, X.; Duan, J.; Xu, X.; Zhang, L. Highly Efficient One-Step Purification of Sulfated Polysaccharides via Chitosan Microspheres Adsorbents. ACS Sustainable Chem. Eng. 2017, 5 (4), 3195–3203.
- (8) Men, J.; Guo, J.; Zhou, W.; Dong, N.; Pang, X.; Gao, B. Preparation of cationic functional polymer poly-(Acryloxyethyltrimethyl ammonium chloride)/SiO2 and its adsorp-

- tion characteristics for heparin. Korean J. Chem. Eng. 2017, 34 (7), 1889–1895.
- (9) Spina, R. L.; Tripisciano, C.; Mecca, T.; Cunsolo, F.; Weber, V.; Mattiasson, B. Chemically modified poly(2-hydroxyethyl methacrylate) cryogel for the adsorption of heparin. *J. Biomed. Mater. Res., Part B* **2014**, *102* (6), 1207–1216.
- (10) Wassell, D. T. H.; Embery, G. Adsorption of chondroitin-4-sulphate and heparin onto titanium: effect of bovine serum albumin. *Biomaterials* **1997**, *18* (16), 1121–1126.
- (11) Eskandarloo, H.; Arshadi, M.; Enayati, M.; Abbaspourrad, A. Highly Efficient Recovery of Heparin Using a Green and Low-Cost Quaternary Ammonium Functionalized Halloysite Nanotube. ACS Sustainable Chem. Eng. 2018, 6 (11), 15349–15360.
- (12) Eskandarloo, H.; Arshadi, M.; Abbaspourrad, A. Magnetic Dendritic Halloysite Nanotube for Highly Selective Recovery of Heparin Digested from Porcine Intestinal Mucosa. ACS Sustainable Chem. Eng. 2018, 6 (11), 14561–14573.
- (13) Du, X.; Hao, X.; Wang, Z.; Guan, G. Electroactive ion exchange materials: current status in synthesis, applications and future prospects. J. Mater. Chem. A 2016, 4 (17), 6236–6258.
- (14) Lin, Y.; Zhou, Q.; Tang, D.; Niessner, R.; Yang, H.; Knopp, D. Silver Nanolabels-Assisted Ion-Exchange Reaction with CdTe Quantum Dots Mediated Exciton Trapping for Signal-On Photoelectrochemical Immunoassay of Mycotoxins. *Anal. Chem.* **2016**, *88* (15), 7858–7866.
- (15) Meng, F.; Liang, W.; Sun, H.; Wu, L.; Gong, X.; Miao, P. A Peptide-Based Electrochemical Biosensor for Facile Measurement of Whole-Blood Heparin. *ChemElectroChem* **2017**, *4* (3), 472–475.
- (16) Fu, X.; Chen, L.; Li, J.; Lin, M.; You, H.; Wang, W. Label-free colorimetric sensor for ultrasensitive detection of heparin based on color quenching of gold nanorods by graphene oxide. *Biosens. Bioelectron.* **2012**, 34 (1), 227–231.
- (17) Wang, X.; Chen, L.; Fu, X.; Chen, L.; Ding, Y. Highly Sensitive Surface-Enhanced Raman Scattering Sensing of Heparin Based on Antiaggregation of Functionalized Silver Nanoparticles. *ACS Appl. Mater. Interfaces* **2013**, *5* (21), 11059–11065.
- (18) Miyazu, K.; Kawahara, D.; Ohtake, H.; Watanabe, G.; Matsuda, T. Luminal surface design of electrospun small-diameter graft aiming at in situ capture of endothelial progenitor cell. *J. Biomed. Mater. Res., Part B* **2010**, *94B* (1), 53–63.
- (19) Foo, K. Y.; Hameed, B. H. A short review of activated carbon assisted electrosorption process: An overview, current stage and future prospects. *J. Hazard. Mater.* **2009**, *170* (2), 552–559.
- (20) Chen, G. Electrochemical technologies in wastewater treatment. Sep. Purif. Technol. 2004, 38 (1), 11–41.
- (21) Rajeshwar, K.; Ibanez, J. G. Environmental Electrochemistry: Fundamentals and Applications in Pollution Sensors and Abatement; Elsevier Science, 1997.
- (22) Kalaruban, M.; Loganathan, P.; Kandasamy, J.; Naidu, R.; Vigneswaran, S. Enhanced removal of nitrate in an integrated electrochemical-adsorption system. *Sep. Purif. Technol.* **2017**, *189*, 260–266.
- (23) Brillas, E.; Martínez-Huitle, C. A. Decontamination of wastewaters containing synthetic organic dyes by electrochemical methods. An updated review. *Appl. Catal., B* **2015**, *166–167*, 603–643.
- (24) Mor, G. K.; Varghese, O. K.; Paulose, M.; Shankar, K.; Grimes, C. A. A review on highly ordered, vertically oriented TiO2 nanotube arrays: Fabrication, material properties, and solar energy applications. *Sol. Energy Mater. Sol. Cells* **2006**, *90* (14), 2011–2075.
- (25) Tan, A. W.; Pingguan-Murphy, B.; Ahmad, R.; Akbar, S. A. Review of titania nanotubes: Fabrication and cellular response. *Ceram. Int.* **2012**, 38 (6), 4421–4435.
- (26) Zhou, X.; Nguyen, N. T.; Özkan, S.; Schmuki, P. Anodic TiO2 nanotube layers: Why does self-organized growth occur—A mini review. *Electrochem. Commun.* **2014**, *46*, 157–162.
- (27) Wang, G.; Feng, H.; Hu, L.; Jin, W.; Hao, Q.; Gao, A.; Peng, X.; Li, W.; Wong, K.-Y.; Wang, H.; Li, Z.; Chu, P. K. An antibacterial platform based on capacitive carbon-doped TiO2 nanotubes after

- direct or alternating current charging. Nat. Commun. 2018, 9 (1), 2055.
- (28) Ming, H.; Ming, J.; Li, X.; Zhou, Q.; Wang, H.; Jin, L.; Fu, Y.; Adkins, J.; Zheng, J. Hierarchical Li4Ti5O12 particles co-modified with C&N towards enhanced performance in lithium-ion battery applications. *Electrochim. Acta* 2014, 116, 224–229.
- (29) Eskandarloo, H.; Selig, M. J.; Abbaspourrad, A. In situ H2O2 generation for de-emulsification of fine stable bilge water emulsions. *Chem. Eng. J.* **2018**, 335, 434–442.
- (30) Ukaji, E.; Furusawa, T.; Sato, M.; Suzuki, N. Appl. Surf. Sci. **2007**, 254, 563-569.
- (31) Cheng, F.; Sajedin, S. M.; Kelly, S. M.; Lee, A. F.; Kornherr, A. UV-stable paper coated with APTES-modified P25 TiO2 nanoparticles. *Carbohydr. Polym.* **2014**, *114*, 246–252.
- (32) Eskandarloo, H.; Hashempour, M.; Vicenzo, A.; Franz, S.; Badiei, A.; Behnajady, M. A.; Bestetti, M. High-temperature stable anatase-type TiO2 nanotube arrays: A study of the structure—activity relationship. *Appl. Catal., B* **2016**, *185*, 119–132.
- (33) Xue, C.; Hu, S.; Chang, Q.; Li, Y.; Liu, X.; Yang, J. Fluoride doped SrTiO3/TiO2 nanotube arrays with a double layer walled structure for enhanced photocatalytic properties and bioactivity. *RSC Adv.* **2017**, *7* (78), 49759–49768.
- (34) Bauer, S.; Park, J.; Mark, K. V. D.; Schmuki, P. Improved attachment of mesenchymal stem cells on super-hydrophobic TiO2 nanotubes. *Acta Biomater.* **2008**, *4* (5), 1576–1582.
- (35) Seredych, M.; Mikhalovska, L.; Mikhalovsky, S.; Gogotsi, Y. Adsorption of Bovine Serum Albumin on Carbon-Based Materials. C 2018, 4 (1), 3.
- (36) Wanci, S.; Shizhu, W.; Naizhen, C.; Lu, Z.; Wei, Z.; Yingjie, L.; Jialin, G. Expanded graphite—a new kind of biomedical material. *Carbon* **1999**, 37 (2), 356–358.
- (37) Bozzini, B.; De Gaudenzi, G. P.; Serra, M.; Fanigliulo, A.; Bogani, F. Corrosion behaviour of WC-Co based hardmetal in neutral chloride and acid sulphate media. *Mater. Corros.* **2002**, *53* (5), 328–334
- (38) Prévot, M. S.; Sivula, K. Photoelectrochemical Tandem Cells for Solar Water Splitting. *J. Phys. Chem. C* **2013**, *117* (35), 17879–17893.
- (39) Aguila, B.; Sun, Q.; Perman, J. A.; Earl, L. D.; Abney, C. W.; Elzein, R.; Schlaf, R.; Ma, S. Efficient Mercury Capture Using Functionalized Porous Organic Polymer. *Adv. Mater.* **2017**, 29 (31), 1700665.
- (40) Tan, I. A. W.; Ahmad, A. L.; Hameed, B. H. Adsorption isotherms, kinetics, thermodynamics and desorption studies of 2,4,6-trichlorophenol on oil palm empty fruit bunch-based activated carbon. *J. Hazard. Mater.* **2009**, *164* (2), 473–482.
- (41) Doğan, M.; Abak, H.; Alkan, M. Adsorption of methylene blue onto hazelnut shell: Kinetics, mechanism and activation parameters. *J. Hazard. Mater.* **2009**, *164* (1), 172–181.
- (42) Atkins, P.; de Paula, J. Atkins' Physical Chemistry, 7th ed.; Oxford University Press, 2002; p 1149
- (43) Li, J.; Hou, Y.; Chen, X.; Ding, X.; Liu, Y.; Shen, X.; Cai, K. Recyclable heparin and chitosan conjugated magnetic nanocomposites for selective removal of low-density lipoprotein from plasma. *J. Mater. Sci.: Mater. Med.* **2014**, 25 (4), 1055–1064.
- (44) Bhaskar, U.; Hickey, A. M.; Li, G.; Mundra, R. V.; Zhang, F.; Fu, L.; Cai, C.; Ou, Z.; Dordick, J. S.; Linhardt, R. J. A purification process for heparin and precursor polysaccharides using the pH responsive behavior of chitosan. *Biotechnol. Prog.* **2015**, *31* (5), 1348–1359.
- (45) Lalhruaitluanga, H.; Jayaram, K.; Prasad, M. N. V.; Kumar, K. K. Lead(II) adsorption from aqueous solutions by raw and activated charcoals of Melocanna baccifera Roxburgh (bamboo)—A comparative study. J. Hazard. Mater. 2010, 175 (1), 311–318.
- (46) Doğan, M.; Alkan, M.; Demirbaş, Ö.; Özdemir, Y.; Özmetin, C. Adsorption kinetics of maxilon blue GRL onto sepiolite from aqueous solutions. *Chem. Eng. J.* **2006**, *124* (1), 89–101.

- (47) Langmuir, I. THE ADSORPTION OF GASES ON PLANE SURFACES OF GLASS, MICA AND PLATINUM. *J. Am. Chem. Soc.* **1918**, *40* (9), 1361–1403.
- (48) Yan, Z.; Li, G.; Mu, L.; Tao, S. Pyridine-functionalized mesoporous silica as an efficient adsorbent for the removal of acid dyestuffs. *J. Mater. Chem.* **2006**, *16* (18), 1717–1725.
- (49) Yoon, S. W.; Shim, H. J.; Shim, I.-B. Improving the Osteoblast Cell Adhesion on Electron Beam Controlled TiO2 Nanotubes. *J. Nanomater.* **2014**, *7*, 1.
- (50) Seo, H. Y.; Kwon, J.-S.; Choi, Y.-R.; Kim, K.-M.; Choi, E. H.; Kim, K.-N. Cellular Attachment and Differentiation on Titania Nanotubes Exposed to Air- or Nitrogen-Based Non-Thermal Atmospheric Pressure Plasma. *PLoS One* **2014**, *9* (11), No. e113477.
- (51) Ungvári, K.; Pelsöczi, I. K.; Kormos, B.; Oszkó, A.; Rakonczay, Z.; Kemény, L.; Radnai, M.; Nagy, K.; Fazekas, A.; Turzó, K. Effects on titanium implant surfaces of chemical agents used for the treatment of peri-implantitis. *J. Biomed. Mater. Res., Part B* **2010**, 94B (1), 222–229.
- (52) Meroni, D.; Lo Presti, L.; Di Liberto, G.; Ceotto, M.; Acres, R. G.; Prince, K. C.; Bellani, R.; Soliveri, G.; Ardizzone, S. A Close Look at the Structure of the TiO2-APTES Interface in Hybrid Nanomaterials and Its Degradation Pathway: An Experimental and Theoretical Study. J. Phys. Chem. C 2017, 121 (1), 430–440.
- (53) Cabán-Huertas, Z.; Ayyad, O.; Dubal, D. P.; Gómez-Romero, P. Aqueous synthesis of LiFePO4 with Fractal Granularity. *Sci. Rep.* **2016**, *6*, 27024.
- (54) Ceotto, M.; Lo Presti, L.; Cappelletti, G.; Meroni, D.; Spadavecchia, F.; Zecca, R.; Leoni, M.; Scardi, P.; Bianchi, C. L.; Ardizzone, S. About the Nitrogen Location in Nanocrystalline N-Doped TiO2: Combined DFT and EXAFS Approach. *J. Phys. Chem.* C 2012, 116 (2), 1764–1771.
- (55) Eskandarloo, H.; Badiei, A. Fabrication of an inexpensive and high efficiency microphotoreactor using CO2 laser technique for photocatalytic water treatment applications. *Environ. Technol.* **2015**, 36 (8), 1063–1073.
- (56) Eskandarloo, H.; Zaferani, M.; Kierulf, A.; Abbaspourrad, A. Shape-controlled fabrication of TiO2 hollow shells toward photocatalytic application. *Appl. Catal.*, B **2018**, 227, 519–529.
- (57) Zhuang, J.; Tang, D.; Lai, W.; Xu, M.; Tang, D. Target-Induced Nano-Enzyme Reactor Mediated Hole-Trapping for High-Throughput Immunoassay Based on a Split-Type Photoelectrochemical Detection Strategy. *Anal. Chem.* **2015**, 87 (18), 9473–9480.
- (58) Beyer, T.; Matz, M.; Brinz, D.; Rädler, O.; Wolf, B.; Norwig, J.; Baumann, K.; Alban, S.; Holzgrabe, U. Composition of OSCS-contaminated heparin occurring in 2008 in batches on the German market. *Eur. J. Pharm. Sci.* **2010**, 40 (4), 297–304.